Journal of Engineering Science and Technology
Vol. 13, No. 3 (2018) 704 - 714

EVALUATION OF ITERATIVE INTERPOLATION METHODS FOR METAL ARTEFACTS REDUCTION OF PELVIC COMPUTED TOMOGRAPHY IMAGES: A PHANTOM STUDY

TITIPONG KAEWLEK

Department of Radiological Technology, Faculty of Allied Health Sciences,
Naresuan University, 65000, Phitsanulok, Thailand
*E-mail: titipongk@nu.ac.th

Abstract

Metal artefacts obscure the organs as shown on a computed tomography (CT) image. The effect of the artefact can be reduced by using sinogram completion techniques. The aim of this study is to evaluate interpolation methods - linear interpolation (LI), total variation in painting (TV), high order total variation inpainting (HTV) for reducing the effect of the artefact. In this study, the sinogram completion technique applied on the simulated pelvic CT image of a hip prosthesis. Algorithms consist of four steps: 1) segment the metal region on the image, 2) transform the image into a sinogram and find the boundary of the metal sinogram, 3) estimate the new value of the missing data using three different methods 4) reconstruct the modified sinogram and add back the metal region into the reconstructed image. The percentages of the difference of intensity value between the artefact image and the non-artefact image of three techniques were computed. The percentages of artefact reduction were evaluated to compare the effectiveness of algorithms. The HTV method can provide the lowest difference of intensity value amongst three interpolation algorithms. The artefact reduction of the HTV method reduced 89.43%. The HTV technique could be used for solving the metal artefact problem effectively on CT images.

Keywords: Metal artefact reduction, Sinogram completion, Iterative interpolation, CT image.

1. Introduction

One problem of the computed tomography (CT) imaging is the effect of artefacts. Artefacts can degrade the image quality and effect diagnosis. Artefacts may include

Nomenclatures

D	The region to be inpainted
E	The outer neighbourhood of D
$f(x)$	Target value
F	A called double-well potential
I_{ini}	The initial image
I_m	Metal image
I_{MAR}	Metal artefacts reduction image
I_R	Image reconstruction of modified sinogram
J	The value of energy function
$RSME_{\text{i}}$	Root mean square error of the artefact image
$RSME_r$	Root mean square error of the reduced artefact image
$S_m(u, \theta)$	Metal sinogram image
$S_T(u, \theta)$	Thresholded sinogram image
Th, T	Threshold value
u, u_t	The target pixel value

Greek Symbols

∇u	The gradient of u
λ	A fitting constant or Lagrange multiplier
Ω	Metal regions.

Abbreviations

AI	Artefact image
CT	Computed tomography
HTV	High order total variation inpainting
LI	Linear interpolation
NI	Non-artefact image
ROIs	Region of interest
TV	Total variation inpainting
RMSE	Root mean square error
ROIs	Region of interest

noise, motion and metal artefacts. Metal artefacts are the most common cause of disturbed CT images. These artefacts frequently occur when scanning patients with prosthetic implants. Medical implants may be prosthetic implants for supportive treatment or for the treatment of a health problem. Examples of implants include screws or rods for spinal treatment, dental fillings or dental implants, stents for vascular support, metal clips for the treatment of cerebral thrombosis and prostheses for joint replacement [1].

In the case of hip prostheses, a dark band obscures the critical organs between the sides of the prosthesis and the surrounding streak effect radiates into the surrounding area, obscuring the organs and tissues [2-3]. A way to reduce the effect of the artefact is the technique of adjusting the parameters, for example, adjust the tube current and voltage, and reconstruct the image to multiplannar [4]. Another method is the applied algorithms - iterative reconstruction [5]. Sinogram completion methods may also be used [6-8]. Iterative reconstruction is the best

way to eliminate the effect of artefacts, but it takes more time. Thus, the sinogram completion method is considered to be an appropriate method to reduce these effects. One of the procedures of metal artefact reduction is the estimated sinogram to complete the missing value using the linear interpolation technique. This technique induced the effects of the artefacts, something that needs to be avoided. Iterative interpolation is the means to correct this error. The verification of the iterative interpolation technique was examined.

This paper compares three iterative interpolation techniques; total variation inpainting (TV), high order total variation inpainting (HTV) and the traditional (linear interpolation) method. The algorithms applied to the simulation of phantom images and used to measure the qualitative image quality.

2. Materials and Methods

2.1. Materials

Phantom simulation

In this study, a pelvic phantom image was simulated and a prosthetic hip replacement was inserted on both sides of the pelvis. A computer simulation generated the metal artefact (streak artefact and dark bands). The simulated prostheses were divided into two groups: one side and both sides of the pelvis. The phantom was modified from the shepp-logan phantom data [9]. The intensity value of the phantom are 0-255 (the image data is an 8 bit image).

2.2. Methods

The main algorithm is the sinogram completion method. This study tested three algorithms to reduce the streak artefact and dark bands in CT images. Three interpolation algorithms were compared to test the performance in the estimation of new data processes.

The metal artefact reduction method consists of four steps:

(i) *Implant identification*: to determine the shape of the metal objects on the initial image, the image data are segmented (intensity value) into two groups; soft tissue and metal. The image data are identified as belonging to the soft tissue regions and the metal regions by simple thresholding, as follows:

$$I_m(x,y) = \begin{cases} 0 & for\ (x,y) \notin \Omega \\ \Omega(x,y) & for\ (x,y) \in \Omega \end{cases} \quad (1)$$

where $I_m\ (x,\ y)$ is metal image, $\Omega = \{(x,\ y)|\ I_{ini}(x,\ y) > Th\}$, Ω is metal regions, $I_{ini}(x, y)$, is the initial image, Th is threshold value.

After metal segmentation, the soft tissue regions and the metal regions are transformed into sinogram domains.

(ii) *Metal sinogram segmentation*: the global thresholding method [10] is algorithms to identify the suitable boundary of the metal on metal sinogram as follows:

$$S_T(u,\theta) = \begin{cases} 1 & if\ S_m(u,\theta) \geq T \\ 0 & otherwise \end{cases} \quad (2)$$

where T is the threshold value, $S_m(u, \theta)$ is the metal sinogram image, $S_T(u, \theta)$ is the thresholded sinogram image.

(iii) *Estimation of the missing data on the soft tissue sinogram*: to calculate the new value of the missing data from the thresholded sinogram, the three algorithms are used.

(a) The linear interpolation technique: linear interpolation is the straight line between the two known co-ordinate points. Calculate the interpolated value using Eq. (3).

$$f(x) = f(x_0) + \frac{f(x_1) - f(x_0)}{x_1 - x_0}(x_1 - x_0) \tag{3}$$

where, $f(x)$ is the target value, $f(x0)$ are first co-ordinates, and $f(x1)$ are second co-ordinates.

(b) The total variation inpainting (TV) technique: the missing data was estimated to complete the sinogram by TV inpainting [11] as follows:

$$J(u, D) = \int_{D \cup E} |\nabla u| \, dx \, dy + \frac{\lambda}{2} \int_E |u - u_0|^2 \, dx \, dy \tag{4}$$

where D is the region to be inpainted, and E is the outer neighbourhood of D, u is the target pixel value, ∇u is the gradient, λ is a fitting constant or Lagrange multiplier, J is the value of energy function. The TV inpainting model is to minimize.

The Euler-Lagrange equation of the TV inpainting energy is given by

$$-\nabla g\left(\frac{\nabla u}{|\nabla u|}\right) + \lambda_e(u - u_0) = 0\,, \qquad \lambda_e = \begin{cases} \lambda, (x, y) \in E \\ 0, (x, y) \in D \end{cases} \tag{5}$$

(c) The high order total variation inpainting (HTV) technique: Cahn-Hilliard inpainting [12] was used for reading the sinogram data by Eq. (6) and the convexity splitting of second order total variation inpainting used to smooth monotone regularizations on the data between the missing data on soft tissue sinogram data in Eq. (7) with $0<\delta\ll 1$, the details of the HTV are explained in [13].

$$\begin{cases} u_t = \Delta\left(-\epsilon\Delta u + \frac{1}{\epsilon}F'(u)\right) + \lambda(f - u) & in\ \Omega \\ u = f, -\epsilon\Delta u + \frac{1}{\epsilon}F'(u) = 0 & on\ \delta\Omega \end{cases} \tag{6}$$

$$u_t = -\Delta\nabla \cdot \left(\frac{\nabla u}{\sqrt{|\nabla u|^2 - \delta^2}}\right) + \lambda(f - u) \tag{7}$$

$$\lambda(x) = \begin{cases} \lambda_0 & \Omega/D \\ 0, & D \end{cases} \tag{8}$$

where u_t is the region to be inpainted, $F(u)$ is called double-well potential, $F(u) = u^2(u-1)^2$, f is the given sinogram image defined on a sinogram domain, Ω. u is the target pixel value, ∇u is the gradient, λ is a fitting constant in Eq. (8).

(d) *Image reconstruction*: a modified sinogram is then reconstructed by using filtered back-projection. Finally, the metal regions of the original metal class image are added back to complete the modified image.

$$I_{MAR}(x, y) = I_R(x, y) \cup I_{mt}(x, y). \quad (9)$$

where $I_{MAR}(x, y)$ is a metal artefact reduction image, $I_R(x, y)$ is image reconstruction of a modified sinogram, $I_{mt}(x, y)$ is metal region image.

2.3. Evaluation of effectiveness of algorithms

To verify the algorithms, the intensity value was measured and calculated the percentages of difference on the simulation phantom images. The root mean square error between the artefact image and the reduced artefact image of the three algorithms was calculated. The percentages of artefact reduction were also calculated.

2.3.1. Intensity value measurement and the percentages of difference calculation

The region of interest (ROIs) on 1) the streak artefact area beside the hip prosthesis, 2) the dark band between the hip prosthesis, 3) the low-density object and 4) the high-density object in order to measure the intensity value were pressed, Fig. 1(a). In the case of critical organ phantom, the intensity value at 1) the streak artefact area beside the hip prosthesis, 2) the dark band between the hip prosthesis, 3) the bladder and 4) the rectum position were measured, Fig. 1(b).

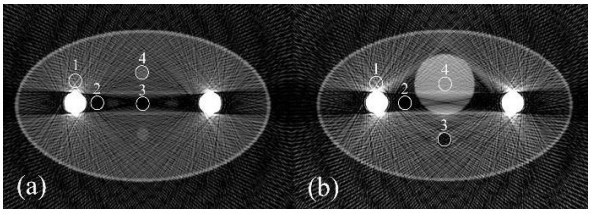

Fig. 1. The regions of interest (ROIs) for measurement of the intensity value.

The percentages of difference of the intensity value between the artifact image or the reduced artefact image and the non-artefact image of three techniques were computed by Eq. (10),

$$\text{The percentages of difference of intensity value} = \left(\frac{|\text{AI-NI}|}{\text{NI}}\right) \times 100. \quad (10)$$

where AI is the intensity value of the artefact image or the reduced artefact image, NI is the intensity value of non-artefact images.

2.3.2. The root mean square error (RMSE) measurement and the percentages of artefact reduction calculation

To evaluate the RMSE of the simulation images, a reference image (non-artefact: $r(x, y)$) was compared with a test image $t(x, y)$. The two images must have the same size $[n_x, n_y]$. The RMSE [14] are calculated as Eq. (11).

$$RMSE = \sqrt{\frac{1}{n_x n_y}\sum_0^{n_x-1}\sum_0^{n_y-1}[r(x,y)-t(x,y)]^2}. \quad (11)$$

The percentages of artefact reduction was calculated by Eq. (12),

$$\text{The percentages of artefact reduction} = \left(\frac{\text{RMSE}_\text{r}\text{-RSME}_\text{i}}{\text{RSME}_\text{i}}\right) \times 100. \quad (12)$$

where, RSME_i is the root mean square error of the artefact image, RSME_r is the root mean square error of the reduced artefact image.

3. Results

Figures 2 and 3 display the three algorithms that can reduce the artefact, both of the small rod phantom and the critical organ phantom images.

Figure 2 shows the result of metal artefact reduction by three different algorithms (LI, TV and HTV) on the phantom inserted small rod. a) The non-artefact images (NI) of one side prosthesis, b) the artefact images (AI) of one side prosthesis, c, d and e) the reduced artefact image by LI, TV and HTV algorithms respectively. f) The non-artefact images (NI) of both sides prostheses, g) the artefact images (AI) of both sides prostheses, h, i and j) the reduced artefact image by LI, TV and HTV algorithms respectively.

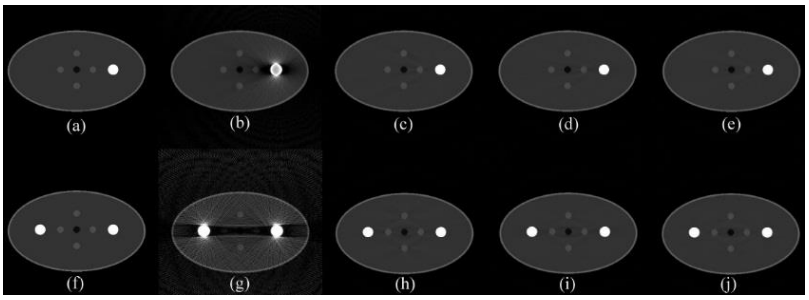

Fig. 2. The result of metal artefact reduction by three different algorithms (LI, TV and HTV) on the phantom inserted small rod.

Figure 3 shows the result of metal artefact reduction by three different algorithms (LI, TV and HTV) on the phantom with critical organs (bladder and rectum). a) The non-artefact images (NI) of one side prosthesis, b) the artefact images (AI) of one side prosthesis, c, d and e) the reduced artefact image by LI, TV and HTV algorithms respectively. f) The non-artefact images (NI) of both sides prostheses, g) the artefact images (AI) of both sides prostheses, h, i and j) the reduced artefact image by LI, TV and HTV algorithms respectively.

In the case of the critical organ phantom, LI created a new artefact beside the hip prosthesis (Fig. 3(c, h)) more than the result image of TV (Fig. 3(d, i)). The HTV significantly, appeared smoother than LI and TV (Fig. 3(e, j)). The artefact reduction of the small rod phantom of HTV algorithms appeared smooth, similar to LI and TV (Fig. 2).

In the streak artefact area, dark band, the low-density object or bladder region and the high-density object or rectum regions, the qualitative analysis (Tables 1 and

2), shows that the intensity value of the HTV algorithm was close to the non-artefact image value. In the case of a small rod phantom, the intensity value of the LI image was closer to the non-artefact image value than TV and HTV. In the streak artefact (the one side prosthesis) area, the low-density object (the one and both sides prosthesis) areas, and the bladder area of critical organ phantom (the one side prosthesis) the LI image was closer to the non-artefact image value than TV and HTV. In the case of small rod phantoms, the intensity value of TV was closer to the non-artefact image value than LI and HTV at the streak artefact (prosthesis on both sides) area and the low-density object (the one side prosthesis) area.

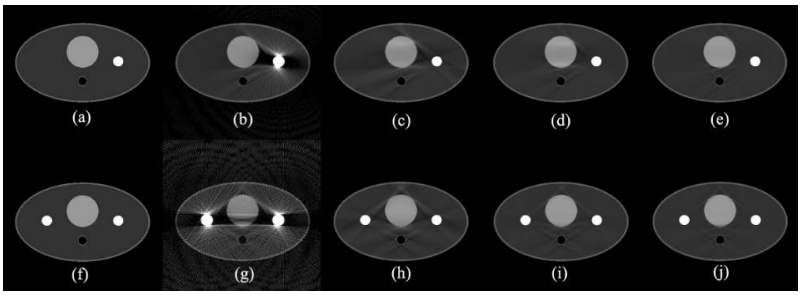

Fig. 3. The result of metal artefact reduction by three different algorithms (LI, TV and HTV) on the phantom with critical organs (bladder and rectum).

Table 1. The percentages of intensity value difference of three different methods on the streak artefact and dark band.

Streak			NI	AI	LI	TV	HTV
Small rod	1 side	Intensity	51.00	107.68	50.98	51.43	49.84
		% difference		111.13	0.04	0.85	2.28
	Both sides	Intensity	51.00	82.93	50.29	51.03	49.76
		% difference		62.61	1.39	0.06	2.44
Critical organ	1 side	Intensity	51.00	118.33	43.18	46.98	49.10
		% difference		132.02	15.34	7.88	3.73
	Both sides	Intensity	51.00	118.30	50.09	50.86	51.11
		% difference		131.96	1.78	0.27	0.22
Dark Band			NI	AI	LI	TV	HTV
Small rod	1 side	Intensity	51.00	5.35	49.46	47.93	50.83
		% difference		89.50	3.03	6.03	0.33
	Both sides	Intensity	51.00	3.29	35.87	43.11	48.79
		% difference		93.55	29.67	15.46	4.33
Critical organ	1 side	Intensity	51.00	7.77	49.48	47.70	50.35
		% difference		84.76	2.98	6.47	1.28
	Both sides	Intensity	51.00	7.50	42.15	46.85	49.35
		% difference		85.30	17.35	8.14	3.23

NI is a non-artefact image, AI is an artefact image, LI is the reduced artefact image of the LI technique, TV is the reduced artefact image of the TV technique, and HTV is the reduced artefact image of the HTV technique.

Table 2. The percentages of intensity value difference of three different methods on the low and high density objects.

Low-density objects / Rectum			NI	AI	LI	TV	HTV
Small rod	1 side	Intensity	12.86	5.86	12.54	11.26	11.37
		% difference		54.40	2.47	12.43	11.56
	Both sides	Intensity	12.86	3.13	13.07	12.06	10.48
		% difference		75.66	1.66	6.20	18.54
Critical organ	1 side	Intensity	6.46	7.42	4.68	4.63	4.47
		% difference		14.87	27.45	28.23	30.80
	Both sides	Intensity	6.46	19.10	4.63	4.58	4.59
		% difference		195.91	28.26	29.12	28.92
High-density objects / Bladder			**NI**	**AI**	**LI**	**TV**	**HTV**
Small rod	1 side	Intensity	77.30	71.34	74.34	75.05	75.16
		% difference		7.71	3.83	2.92	2.77
	Both sides	Intensity	77.30	69.33	72.35	74.02	74.60
		% difference		10.31	6.40	4.24	3.49
Critical organ	1 side	Intensity	153.00	138.24	138.08	139.51	148.24
		% difference		9.64	9.75	8.82	3.11
	Both sides	Intensity	153.00	129.76	153.62	152.38	152.33
		% difference		15.19	0.41	0.40	0.44

NI is a non-artefact image, AI is an artefact image, LI is the reduced artefact image of the LI technique, TV is the reduced artefact image of the TV technique, and HTV is the reduced artefact image of the HTV technique.

Table 3 shows the comparison of the RMSE between the artefact images and the reduced artefact images of the critical organs phantom. The efficiency of HTV algorithms can significantly reduce metal artefacts better than LI and TV algorithms. In the case of small rod phantoms, HTV algorithms of one side and both side of the prosthesis, artefact decreased 68.54% and 85.09 % respectively. In the case of critical organ phantoms, artefact decreased 77.48 % and 89.43 % respectively.

Table 3. The percentages of artefact reduction for the three different methods.

RMSE		**AI**	**LI**	**TV**	**HTV**
Phantom inserted small rod	1 side	11.76	3.77	3.76	3.70
	% Artefact reduction		-67.94	-68.03	-68.54
	Both sides	28.11	4.31	4.30	4.19
	% Artefact reduction		-84.67	-84.70	-85.09
Phantom with critical organ	1 side	17.05	5.25	4.44	3.84
	% Artefact reduction		-69.21	-73.96	-77.48
	Both sides	38.40	5.09	4.11	4.06
	% Artefact reduction		-86.74	-89.30	-89.43

AI is the artefact image, LI is the reduced artefact image of the LI technique, TV is the reduced artefact image of the TV technique, and HTV is the reduced artefact image of the HTV technique.

4. Discussion

In this study, metal artefact reduction was demonstrated by using the sinogram completion method. We compared three algorithms (LI, TV and HTV) for interpolation of the missing data of the sinogram of the artefact image after finding the boundary of the metal sinogram. Linear interpolation (LI) is a simple method to estimate the new straight line between the two known co-ordinates. Total variation inpainting (TV) is an iterative interpolation method for image denoising or image restoring [11]. TV was applied to compute the value with the curve model. The curve line appeared between the two co-ordinates and created smoother sinogram data than the LI method. High order total variation inpainting (HTV) is an iterative interpolation method. In this work, second order variation inpainting was applied to smooth the sinogram data with convexity splitting [12-13]. The sinogram data of HTV algorithms was smoother than LI and TV.

The reconstructed image of the three algorithms, the intensity value of the HTV algorithm image were close to the non-artefact image, and appeared in the new artefact less than LI and TV. Many previous studies [7, 15-17] reduced metal artefact, providing a consistent improvement in image data and depressed the effect of the artefact on critical organs. The linear interpolation remained in many of these studies - a drawback is the new artefact [6, 8, 18].

The limitations of the iterative interpolation method may be that it is more time consuming than linear interpolation. The time of the LI algorithm was 0.084 seconds, TV was 217.08 seconds, and HTV was 128.26 seconds. The time of the iteration method (TV and HTV) about 2000 times and 1000 times, respectively and related to the work of Zhang et al. [16]. The compared time of TV was 1.69 times of HTV algorithm. The suggestion of iterative interpolation can reduce the metal artefacts and can improve image quality. The choice of the high effective energy function could decrease time consumption.

5. Conclusion

The sinogram completion method is an important and well-studied method to reduce metal artefacts. The interpolation algorithms are procedures and precise ways for estimating the value of the missing data of the sinogram domain of computed tomography imaging. This paper compared three interpolation algorithms (LI, TV and HTV) for reducing artefacts on simulated phantom images. The HTV algorithm can create a smooth image and fewer new artefacts appeared beside the hip prosthesis. This is an improvement on LI and TV. The intensity values of the reduced artefact images of the HTV algorithm was also close to the non-artefact image values. The HTV algorithm appears to be efficient in reducing artefact.

Acknowledgments

This study was approved by the institutional review board (IRB) of Naresuan University, Thailand: IRB No. 539/57, COA No. 034/2015 and was supported by

Naresuan University, Thailand (R2559C006). Many thanks also to Mr. Kevin Mark Roebl of the Naresuan University Language Centre for his editing assistance and advice on English expression in this document.

References

1. Vande Berg, B.; Malghem, J.; Maldague, B.; and Lecouvet, F. (2006) Multi-detector CT imaging in the postoperative orthopedic patient with metal hardware. *European Journal of Radiology*, 60, 470-479.
2. Boas, F.E.; and Fleischmann, D. (2012). CT artifacts: causes and reduction techniques. *Imaging in Medicine*, 4(2), 229-240.
3. Barrett, J.F.; and Keat, N. (2004). Artifacts in CT: recognition and avoidance. *Radiographics*, 24, 1679-1691.
4. Kataoka, M.L.; Hochman, M.G.; Rodriguez, E.K.; Lin, P.J.; Kubo, S.; and Raptopolous, V.D. (2010). A review of factors that affect artifact from metallic hardware on multi-row detector computed tomography. *Current Problems in Diagnostic Radiology*, 39,125-136.
5. De Man, B.; Nuyts, J.; Dupont, P.; Marchal, G.; and Suetens, P. (2000). Reduction of metal streak artifacts in x-ray computed tomography using a transmission maximum a posteriori algorithm. *IEEE Transactions on Nuclear Science*, 47(3), 977-981.
6. Bal, M.; and Spies, L. (2006). Metal artifact reduction in CT using tissue-class modeling and adaptive prefiltering . *Medical Physics*, 33(8), 2852 -2859.
7. Chen, Y.; Li, Y.; Guo, H.; Hu, Y.; Luo, L.; Yin, X.; Gu, J.; and Toumoulinand C. (2012). CT metal artifact reduction method based on improved image segmentation and sinogram in - painting. *Mathematical Problems in Engineering*, 1-18. http:// doi:10.1155/2012/786281.
8. Kaewlek, T.; Koolpiruck, D.; Thongvigitmanee, S.; Mongkolsuk, M.; Thammakittiphan, S.; Tritrakarn, S.; and Chiewvit, P. (2015). Metal artifact reduction and image quality evaluation of lumbar spine CT images using metal sinogram segmentation. *Journal of X-Ray Science and Technology*, 23, 649-666.
9. Shepp, L.A.; and Logan, B.F. (1974). The Fourier reconstruction of a head section .*IEEE Transactions on Nuclear Science*, 23, 21-42.
10. Kaewlek, T.; Koolpiruck, D.; Thongvigitmanee, S.; Mongkolsuk, M.; and Chiewvit, P. (2011). Metal artifacts reduction of pedicle screws on spine computed tomography using global thresholding on metal only sinogram . *Proceedings of the 11th Asia-Oceania Congress of Medical Physics and the 6th Japan-Korea Joint Meeting on Medical Physics*, Fukuoka, Kyushu University School of Medicine Centennial Hall Japan.
11. Shen, J.; and Chan, T.F. (2002). Mathematical models for local nontexture inpaintings. *SIAM Journal on Applied Mathematics*, 62(3), 1019-1043.
12. Burger, M.; He, L.; and SchÖnlieb, C.B. (2009). Cahn-Hilliard inpainting and a generalization for gray value images. *The SIAM Journal on Imaging Sciences*, 2(4), 1129-1167

13. SchÖnlieb, C.B.; and Bertozzi, A. (2011). Unconditionally stable schemes for higher order inpainting. *Communications in Mathematical Sciences*, 9(2), 413-457 .
14. Sage, D. (2011). SNR, PSNR, RMSE, MAE: ImageJ's plugin to assess the quality of images .Biomedical Image Group, EPFL, Switzerland . Retrieved May 15, 2015, from http//:bigwww.epfl.ch/sage/soft/snr /
15. Li, Y.; Bao, X.; Yin, X .Chen, Y.; Luo, L.; and Chen, W . (2010). Metal artifact reduction in CT based on adaptive steering filter and nonlocal sinogram inpainting. *Proceedings of 3rd International Conference on Biomedical Engineering and Informatics, IEEE*, Yantai, China, 380-383.
16. Zhang, Y.; Pu, Y.F.; and Ru, J.R. (2011). Fast x-ray CT metal artifacts reduction based on noniterative sinogram inpainting. *IEEE Nuclear Science Symposium Conference Record*, 2462-2464.
17. Zhang, Y.; Pu, Y.F.; Hu, J.R.; Liu, Y.; Chen, Q.L.; and Zhou, J.L. (2011). Efficient CT metal artifact reduction based on fractional-order curvature diffusion. *Computational and Mathematical Methods in Medicine*. 2011,1-9, http://dx.doi.org/10.1155/2011/173748
18. Veldkamp, W.J.H.; Joemai, R.M.S.; van der Molen, A.J.; and Geleijns, J. (2010). Development and validation of segmentation and interpolation techniques in sinograms for metal artifact suppression in CT. *Medical Physics*, 37(2), 620-628.